Patient-Specific Dose and Radiation Risk Estimation in Pediatric Cardiac Catheterization

Klaus Bacher, MSc; Evelien Bogaert, MSc; Régine Lapere, PhD;
Daniël De Wolf, MD, PhD; Hubert Thierens, PhD

Background—Because of the higher radiosensitivity of infants and children compared with adults, there is a need to evaluate the doses delivered to pediatric patients who undergo interventional cardiac procedures. However, knowledge of the effective dose in pediatric interventional cardiology is very limited.

Methods and Results—For an accurate risk estimation, a patient-specific Monte Carlo simulation of the effective dose was set up in 60 patients with congenital heart disease who underwent diagnostic (n=28) or therapeutic (n=32) cardiac catheterization procedures. The dose-saving effect of using extra copper filtration in the x-ray beam was also investigated. For diagnostic cardiac catheterizations, a median effective dose of 4.6 mSv was found. Therapeutic procedures resulted in a higher median effective dose of 6.0 mSv because of the prolonged use of fluoroscopy. The overall effect of inserting extra copper filtration into the x-ray beam was a total effective dose reduction of 18% with no detrimental effect on image quality. An excellent correlation between the dose-area product and effective patient dose was found (r=0.95). Hence, dose-area product is suitable for online estimation of the effective dose with good accuracy. With all procedures included, the resulting median lifetime risk for stochastic effects was 0.08%.

Conclusions—Because of the high radiation exposure, it is important to monitor patient dose by dose-area product instrumentation and to use additional beam filtration to keep the effective dose as low as possible in view of the sensitivity of the pediatric patients. **(*Circulation*. 2005;111:83-89.)**

Key Words: catheterization ■ pediatrics ■ radiation

Interventional cardiology procedures are known to give high radiation doses to patients because of prolonged use of fluoroscopy, multiple cine runs, and the complexity of the procedures.[1–8] The radiation exposure issue in cardiac catheterizations is particularly relevant for infants and children because of their higher radiosensitivity compared with adults, the large fraction of the body irradiated by the x-ray beam, and the probable need to repeat the procedure.[9,10] In addition, cardiac catheterizations are being increasingly used for therapeutic purposes, possibly resulting in higher patient radiation doses.[9–11] When these facts are taken into account, there is a strong need to evaluate the doses delivered to pediatric patients who undergo such high-dose x-ray examinations.[12]

Most of the radiation dosimetry studies performed in pediatric patients are based on measurements with thermoluminescence dosimeters (TLDs) for estimating the dose to the skin, thyroid, and gonads.[12–16] Other studies have indicated the dose-area product (DAP).[10,12,17,18,21] However, to assess the potential risk for stochastic effects such as cancer and leukemia resulting from cardiac catheterization procedures, the effective dose should be calculated.[19] The limited published results are based mainly on phantom measurements or calculated conversion factors and do not take into account the real exposure settings and geometry.[9,20,21]

Therefore, the aim of the present study was to find a patient-specific determination of the effective dose in pediatric heart catheterization procedures and to investigate whether previously reported results on risk estimates are comparable to this patient-specific dosimetry. Furthermore, radiation doses of diagnostic procedures are compared with those of common therapeutic interventions. Because dose reduction in pediatric settings is of great importance, we also investigated the dose-saving effect of using extra copper filtration in the x-ray beam.

Methods

Patients

The patient population included 60 consecutive pediatric patients with congenital heart disease (age ≤10 years). The study group comprised 33 male and 27 female patients with a median age of 2.0 years (range, 1 month to 10 years) and a median weight of 11.7 kg (range, 3.0 to 43 kg). Nineteen patients were <1 year of age. Of the 60 patients, 28 underwent cardiac catheterization procedures for diagnostic purposes (Table 1). Thirty-two patients were referred for a therapeutic catheter procedure: 11 for patent ductus arteriosus

Received May 3, 2004; revision received September 3, 2004; accepted October 15, 2004.

From the Department of Medical Physics and Radiation Protection (K.B., E.B., R.L., H.T.), Ghent University, and the Department of Pediatric Cardiology (D.D.W.), Ghent University Hospital, Gent, Belgium.

Reprint requests to Klaus Bacher, MSc, Ghent University, Department of Medical Physics and Radiation Protection, Proeftuinstraat 86, B-9000 Gent, Belgium. E-mail klaus.bacher@Ugent.be

Circulation **is available at http://www.circulationaha.org** **DOI: 10.1161/01.CIR.0000151098.52656.3A**

TABLE 1. Lesions Studied in the Diagnostic Catheterization Patient Group

Lesions	Patients, n
Univentricular heart	15
Double aortic arch	1
Truncus arteriosus	1
Aortopulmonary collaterals	1
Pulmonary atresia and intact septum	2
Total anomalous pulmonary venous drainage	1
Double discordance	1
Pulmonary atresia and VSD	2
Coronary artery fistula	1
Swiss cheese VSD	1
RV aneurysma	1
AVSD	1

VSD indicates ventricular septal defect; RV, right ventricular; and AVSD, AV septal defect.

occlusion, 10 for atrial septal defect (ASD) closure, and 11 for balloon dilatation. All examinations were carried out by an experienced pediatric cardiologist.

X-Ray System

All studies were performed with an Integris BH5000 biplane x-ray system (Philips) consisting of a frontal Poly Diagnost C2 and a lateral L-arc 2 U. Tube settings such as peak voltage and anode current are controlled by the automatic brightness control. Pulsed fluoroscopy (12.5 frames per second) and cineangiography (25 frames per second) were used.

For fluoroscopy, 2 x-ray beam filtrations were available. The standard setting consisted of a filtration of 1.5 mm Al, combined with 0.2 mm Cu. The low-dose fluoroscopy setting had an extra filtration of 0.2 mm Cu. The half-value layers of the x-ray tubes for both fluoroscopy settings were measured at 80 kVp with a NE2571 Farmer ionization chamber (Thermo Electron, UK). For both tubes, values of 6.2 and 7.3 mm Al were obtained for the standard and low-dose fluoroscopy settings, respectively.

For the measurement of the dose-area product (DAP) at the frontal and lateral tubes, 2 transmission ionization chambers (PTW) were attached to the tube housing of each x-ray tube and connected to a Diamentor M4 readout unit (PTW). DAP meters were calibrated in situ with the NE2571 Farmer ionization chamber and 33×41-cm Kodak X-Omat V films (Eastman Kodak). The calibration factor was taken as the ratio between the actual DAP, calculated as the dose in the center of the field multiplied by the field size measured from the film, and the DAP reading from the Diamentor M4. The calibration was performed for both beam filtration settings, with a peak potential ranging from 50 to 125 kV (Figure 1).

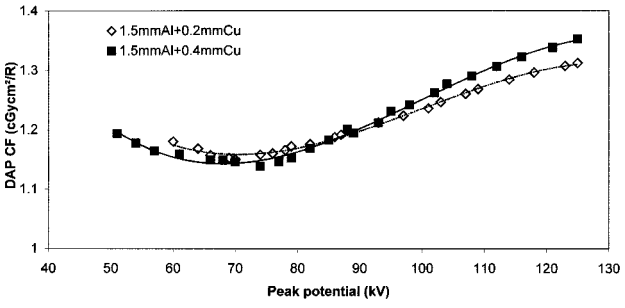

Figure 1. Calibration factor of DAP monitors for frontal x-ray tube. R indicates uncalibrated readout of DAP monitor.

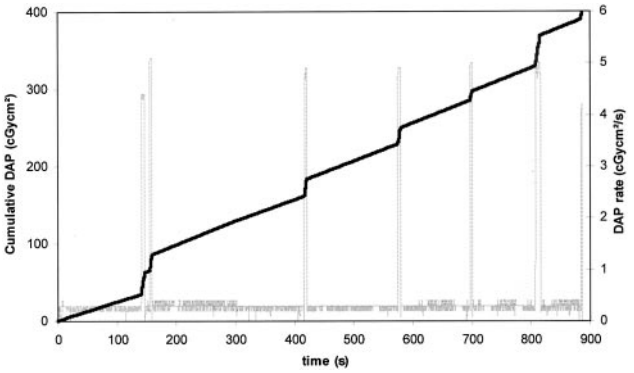

Figure 2. Typical output of DAP registration program. Registered DAP (solid line) and DAP rate (dashed line) as function of time. Example shows output for frontal tube.

Effect of Extra Filtration on Image Quality and Dose

To investigate the dose reduction when an extra 0.2 mm of copper filtration (low-dose setting) was used, patients were randomized to the standard or the low-dose fluoroscopy setting. From the 28 diagnostic catheterizations, 13 were performed with low-dose fluoroscopy and 15 with standard settings. In half of the therapeutic interventions, low-dose fluoroscopy was used. Skin and effective doses were calculated in both groups as described below.

For an objective image quality analysis of the effect of the additional filtration, a CDRAD 2.0 (University of Nijmegen) contrast-detail phantom study was set up.[22] The phantom was used to assess the minimum contrast required to visualize objects of different sizes above the noise threshold.

The phantom was placed between 2 layers of 5-cm PMMA to simulate patient scatter. For both filtration settings, images were acquired in the same conditions as used for patients. All images were scored by 5 independent readers using the methodology as described by the manufacturer.[22] The results are presented in contrast-detail curves.

Acquisition of Exposure Parameters

For each projection used in the cardiac intervention, tube potential, filtration settings, fluoroscopy times, and position of the x-ray tubes were recorded for all patients. The x-ray tube position (rotation and skew), tube potential, source-to-image-intensifier distance, and image intensifier field size were registered automatically for every cine run by the system.

DAP data were gathered by connecting the Diamentor M4 readout unit to a laptop and using software written in-house. In this way, DAP values could be analyzed as a function of time. A distinction could be made between the fluoroscopy and the cine run contributions based on the large difference in DAP rate (cGycm^2/s) between fluoroscopy and cine mode (Figure 2). DAP calibration factors were applied according to the tube potential and the filtration settings of an exposure. Thus, the variation in the DAP calibration factor with beam quality was taken into account.

Skin Dose Measurements

To measure the entrance skin dose from the frontal tube, an array of 14-LiF TLD meters (Harshaw TLD-100, Thermo Electron) was attached to a 33×41 cm Kodak X-Omat V dosimeter film. Afterward, the film was placed on the table underneath the patient's back, near the frontal x-ray tube. The lateral entrance skin dose was assessed by placing 3 TLDs at the right armpit of the patient.

TLDs were analyzed by a Harshaw 3500 reader (Thermo Electron Corp). Optical density readings from the film were obtained with a digital densitometer-scanner (Vidar System Corp).

TABLE 2. Demographic Patient Data and Exposure Parameters Used for Diagnostic Catheterizations

	Diagnostic Catheterizations		
	Standard Fluoroscopy (n=15)	Low-Dose Fluoroscopy (n=13)	*P*
Demographic patient data			
Age, y	2.4 (0.1–8.8)	1.3 (0.1–9.2)	0.695
BMI, kg/m^2	14.6 (12.6–21.6)	14.9 (12.6–21.0)	0.945
Exposure parameters			
Peak voltage frontal tube, kV	77.0 (58.3–79.6)	76.6 (71.2–80.3)	0.818
Peak voltage lateral tube, kV	84.9 (59.5–100.0)	85.7 (74.6–102.0)	0.773
Fluoroscopy time, s	294 (30–870)	234 (96–1992)	0.316
Total DAP, cGycm	548 (114–1461)	337 (96–1399)	0.510
Fluoroscopic DAP rate, cGycm /s	0.61 (0.53–0.92)	0.46 (0.22–0.94)	0.042
PA cine runs, n	4.0 (1–9)	3.0 (1–7)	0.293
LAT cine runs, n	3.0 (0–9)	2.0 (0–6)	0.356

BMI indicates body mass index; PA, postanterior; and LAT, lateral. Values represent the median (range).

All TLDs were calibrated at the same beam quality that was used in situ. The SD within the set of TLDs was minimized to 2%. The X-Omat V film dosimeter was calibrated as described elsewhere.[23]

Film dosimetry was used to verify whether the maximum skin dose measured by TLD corresponded to the maximum skin dose assessed by film. If there was a good correspondence, TLD readings were preferred over film results because of their better accuracy. In addition, the measured skin dose distribution by film dosimetry served as a verification of the results of the dose distributions obtained by Monte Carlo simulation.

Patient-Specific Effective Dose Simulation

The effective dose, introduced by the International Commission on Radiological Protection (ICRP), representative of the risk of late radiation-induced effects as malignancies, is defined by the following expression[19]:

$$E=\sum_T W_T H_T,$$

where H_T is the equivalent dose to tissue T and W_T is the weighting factor representing the relative radiation sensitivity of tissue T. Organ equivalent doses were calculated with the Monte Carlo code MCNP4b2.[24]

The simulations take into account the irradiation geometry of the x-ray tubes and the x-ray spectral distribution used for a particular projection in a patient. X-ray spectra were calculated with an analytical program.[25,26] Field size at the patient's skin level was calculated by measuring the focus-to-skin distance and by using the recorded source-to-image-intensifier distance and the image intensifier field size. The field geometry for fluoroscopy was copied from the first cine run after a series of fluoroscopy. This technique is acceptable because most of the fluoroscopy is used to position the catheter for the next cine run, which is done with the same tube incidence.

Because of the broad differences in body length and weight between the standard pediatric mathematical phantoms of 0, 1, 5, 10, and 15 years,[27] we developed a Visual Basic (Microsoft) program, allowing us to generate a more refined patient-specific phantom based on the gender and the length of the patient. Phantom

TABLE 3. Demographic Patient Data and Exposure Parameters Used for Therapeutic Catheterizations

	Therapeutic Catheterizations		
	Standard Fluoroscopy (n=16)	Low-Dose Fluoroscopy (n=16)	*P*
Demographic patient data			
Age, y	2.0 (0.2–10.0)	2.0 (0.3–7.8)	0.401
BMI, kg/m^2	15.6 (10.1–23.7)	16.3 (13.4–30.1)	0.258
Exposure parameters			
Peak voltage frontal tube, kV	75.0 (56.0–84.8)	79.1 (77.0–91.8)	0.041
Peak voltage lateral tube, kV	83.0 (60.0–96.5)	89.7 (77.0–116)	0.024
Fluoroscopy time, s	401 (182–3612)	300 (42–2466)	0.267
Total DAP, cGycm	472 (282–2044)	272 (41–1800)	0.079
Fluoroscopic DAP rate, cGycm /s	0.71 (0.42–1.11)	0.55 (0.30–0.91)	0.039
PA cine runs, n	3.5 (2–7)	3.0 (2–14)	0.376
LAT cine runs, n	3.5 (0–6)	3.0 (2–13)	0.249

Abbreviations as in Table 2. Values represent the median (range).

calculation was based on the interpolation between the standard pediatric phantoms. In all cases, the arms were removed from the body phantom, simulating the normal clinical practice in which the patients have to move their arms along their head so as not to obstruct the lateral projection. The patient table was also included in the model to compensate for additional attenuation. The x-ray simulation was based on the assumption that the heart lies in the isocenter of the x-ray beams of the C arms.

The computer phantom, the geometry of the x-ray tube, and the x-ray spectrum were used as input for the Monte Carlo simulations. Then, for every tube incidence and for each exposure mode, the effective dose per unit DAP was calculated using the ICRP60 organ weighting factors.[19] For the remainder dose, the mass-weighted average of the remainder organs listed in the latter report was taken. The dose to the bone marrow was calculated with the method of Rosenstein[28] and the published kerma-to-dose conversion factors.[29] The dose to the bone surface was taken as the dose to the skeleton excluding the marrow. By multiplying the effective dose per unit DAP by the corresponding recorded DAP, we could calculate the total effective patient dose. As a verification of the Monte Carlo calculations, the dose distribution at the location of the X-Omat V film was simulated and compared with the distribution derived from the film.

Risk Estimation

The lifetime mortality risk resulting from stochastic effects such as cancer and leukemia was determined by multiplying the effective dose by the appropriate risk factor. In this study, we used the age- and gender-dependent risk factors from the multiplicative model recommended in the ICRP 60 publication: 13%/Sv for boys and 16%/Sv for girls[19] 10 years of age.

Statistical Analysis

Correlations in scatterplots were investigated by calculating the Pearson correlation (r). Differences between 2 independent (not normally distributed) populations were tested for significance with the 2-tailed Mann-Whitney test (95% confidence level). All statistical calculations were performed with the SPSS 10.0.5 program.

Results

Exposure Data

Demographic patient data and exposure parameters used during the cardiac catheterization procedures are summarized in Tables 2 and 3 for the diagnostic and therapeutic interventions, respectively. The data for the 2 patient groups receiving standard and low-dose fluoroscopy are indicated separately. There was no statistical difference in age and body mass index between the patient groups; hence, no bias was introduced as a result of differences between the groups.

The median fluoroscopy time during the cardiac catheterizations was 372 seconds (range, 30 to 3612 seconds). More fluoroscopy was used in therapeutic procedures (median, 456 seconds; range, 42 to 3612 seconds) compared with diagnostic catheterizations (median, 261 seconds; range, 30 to 1992 seconds), but the difference was not statistically significant at the 95% confidence level ($P=0.089$).

Use of the frontal and lateral tubes for cineangiography acquisitions was well balanced. The median measured cumulative DAP was 453 cGycm^2 (range, 41 to 2044 cGycm^2). As a result of the longer fluoroscopy times and slightly higher number of cineangiographies, the median DAP was found to be higher in therapeutic interventions (463 cGycm^2; range, 41 to 2044 cGycm^2) compared with diagnostic procedures (409 cGycm^2; range, 96 to 1461 cGycm^2). However, differences were not statistically significant ($P=0.568$).

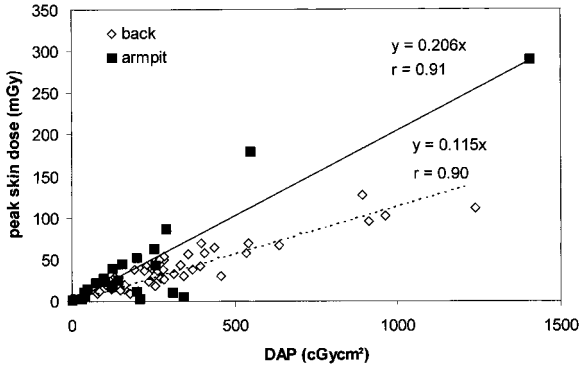

Figure 3. Correlation between maximum lateral and back skin dose measured by TLD and DAP. With extreme value for lateral dose taken out (hot spot >250 mGy), correlation of lateral skin dose and DAP remains good ($r=0.78$, slope=0.203).

The use of 0.2 mm extra copper filtration for fluoroscopy reduced the fluoroscopy DAP rate from a median of 0.71 to 0.51 cGycm^2/s. This 29% reduction was significant ($P=0.041$).

Skin Dose

Peak entrance skin doses measured with the TLD array on the patient's back showed very good agreement with the X-Omat film doses ($r=0.98$). Correspondence between the 2 measurement techniques showed that the TLD array accurately detects the maximum skin dose. The median peak skin dose at the patient's back was 34.2 mGy (range, 12.1 to 144 mGy). The median lateral peak skin dose, measured near the patient's armpit, was 23.9 mGy (range, 1.49 to 297.5 mGy).

A strong correlation was found between DAP and maximum skin dose (Figure 3). This was the case for the frontal ($r=0.90$) and lateral ($r=0.91$) skin exposure. In 4 cases, the lateral TLD dosimeters were clearly not located at the peak skin dose positions.

Effective Dose Simulation

Comparison of the dose distributions measured on film and simulated with MCNP resulted in differences of <7% in all patients.

Median effective doses for diagnostic and therapeutic cardiac interventions are shown in Figure 4. Contributions of cineangiography and fluoroscopy in the total effective dose are indicated in Figure 4A. Figure 4B illustrates the contributions of the frontal and lateral tube exposures to the effective dose.

For the diagnostic cardiac catheterization, the median effective dose was 4.6 mSv (range, 0.6 to 23.2 mSv). The cine contributed a median of 69% to the dose, and 49% of the effective dose was due to exposure of the lateral tube.

The therapeutic cardiological procedures resulted in a median effective dose of 6.0 mSv (range, 1.0 to 37.0 mSv). The cine had a median contribution of 45%, whereas 47% of the effective dose was due to the lateral exposure. ASD closure procedures were subject to a significantly lower effective dose (median, 2.8 mSv; range, 1.8 to 7.4 mSv) compared with the patent ductus arteriosus occlusions (me-

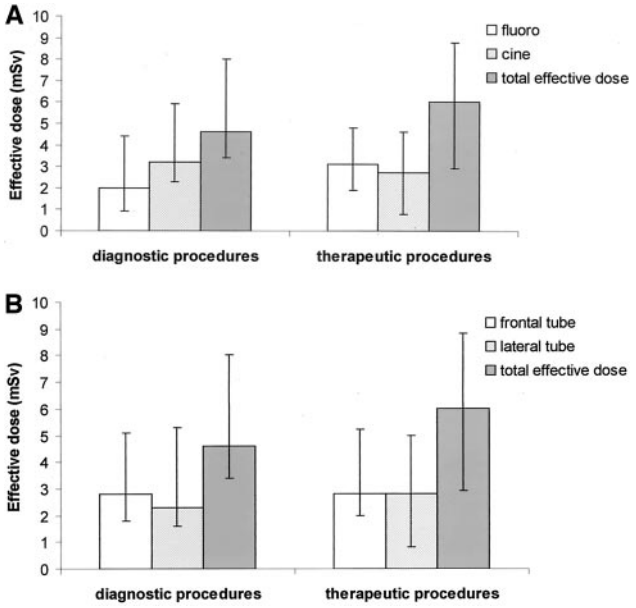

Figure 4. Median effective dose for diagnostic and therapeutic catheterizations. A, Median contributions of fluoroscopy and cineangiography in total effective dose. B, Median contribution of frontal and lateral exposures in effective dose. Error bars represent 25% and 75% percentiles.

dian, 7.6 mSv; range, 2.1 to 37 mSv) and the balloon dilatations (median, 8.1 mSv; range, 2.9 to 20 mSv).

In Figure 5A, the fluoroscopy part of the effective dose is plotted versus fluoroscopy time for standard and low-dose

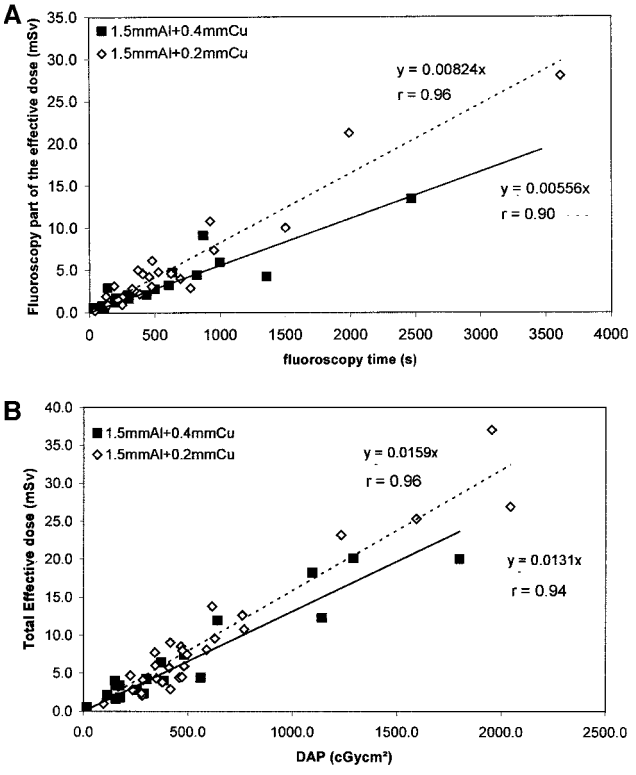

Figure 5. A, Correlation between effective dose resulting from fluoroscopy and fluoroscopy time. B, Correlation between total effective dose and DAP for 2 filtrations considered in this study.

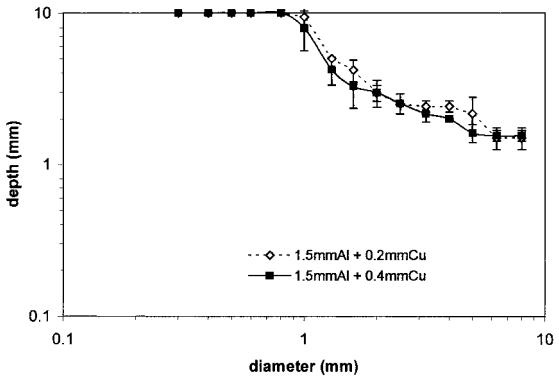

Figure 6. Contrast-detail curve for standard and low-dose filtration settings.

fluoroscopy settings. Application of low-dose fluoroscopy resulted in a mean reduction of the fluoroscopy part of the effective dose of 33%. The overall effect of inserting an extra 0.2 mm copper filtration in the x-ray beam was a total effective dose reduction of 18% (Figure 5B). An excellent correlation between the DAP and the effective patient dose was found for both normal (r=0.96) and low-dose (r=0.94) fluoroscopy.

Image Quality of Low-Dose Fluoroscopy

The contrast-detail study showed no statistically significant difference in low-contrast performance of the standard filtration compared with the low-dose fluoroscopy settings (P=0.437). The contrast-detail curves, averaged over the 5 independent readers, are presented in Figure 6.

Risk Estimation

Including all procedures, the median lifetime risk for stochastic effects was 0.08% (range, 0.007% to 0.481%). The risk estimates for male and female patients did not differ significantly. No significant risk difference was found between therapeutic (median, 0.09%) and diagnostic (median, 0.06%) catheterizations.

The highest effective doses and corresponding risk estimates were found for the youngest patients (<1 year of age). The median lifetime risk for the latter group was 0.10% (range, 0.007% to 0.481%). For the age groups of 2 to 5 years and 6 to 10 years, the median risk was 0.08% (range, 0.016% to 0.431%) and 0.05% (range, 0.030% to 0.320%), respectively.

Discussion

Cardiac catheterizations are among the radiological x-ray procedures with the highest patient radiation dose and therefore are of great concern in pediatric settings because of the higher tissue radiosensitivity of infants and children.[9–15] Moreover, in children with congenital heart disease, there is often a need to perform multiple examinations, increasing the radiation risks.[9,10] About 7% of all cardiac angiography procedures are carried out in children 0 to 15 years of age.[30]

Over the last few years, an increasing number of therapeutic catheterization procedures have been performed in children.[9–11] In general, the justification of these procedures is

evident because they avoid complicated invasive surgery. However, the complexity of these procedures results in higher radiation exposures caused by the longer fluoroscopy times.[9–11] The high patient doses and the introduction of new interventional procedures stress the need for an inventory of the doses delivered to pediatric patients who undergo these high-dose x-ray examinations.[9,12]

The risk for a skin injury is related to the maximum skin dose value.[7] The maximum skin dose measured in this study (297.5 mGy) was far below the 2-Gy threshold level for transient erythema. The median peak skin dose of 34.2 and 23.9 mGy for the anterior-posterior and the lateral exposures, respectively, may be compared with previous (mean) values of 126.2 mGy,[12] 149 mGy,[13] and 74 mGy.[14] Only one study reported a mean entrance skin dose of 481 mGy for children <10 years of age.[15] Because of the moderate values of skin doses in pediatric catheterizations, radiation-induced skin injuries are unlikely. On the other hand, skin dose has to be monitored so that the cardiologist knows the maximum skin dose delivered during the procedure. Because the DAP correlates very well with peak skin dose ($r=0.90$) for the posterior-anterior and lateral exposures, DAP measurement is suitable for online skin dose estimation and may avoid radiation-induced skin injuries in any case. This finding corresponds with a similar correlation found by Boothroyd et al.[12]

In contrast with TLD measurements, DAP monitoring is easily performed, even for very complex procedures. As a result, DAP measurements from pediatric cardiac catheterizations were published in different studies. In our study, the overall measured DAP varied from 41 to 2044 cGycm,^{2} and the median value of 453 cGycm^2 is in good agreement with the results of others.[10,12,17,18,21]

To assess the potential risk for stochastic effects such as cancer and leukemia, the effective dose should be calculated.[19] Unfortunately, determining the effective dose in catheterization procedures is not straightforward, mainly because of the complexity of the x-ray beam geometry (beam direction and field size variations during the catheterization procedure). Moreover, individual anatomy should be taken into account. Anatomy is very important for child dose estimations because patient weights and lengths may be subject to large variations. As a result of these dosimetric complications, data in the literature on the effective dose in pediatric interventional cardiology are scarce. The published results are based mainly on phantom measurements or a restricted number of existing conversion factors without taking into account the real exposure settings and geometry.[9,20,21] Furthermore, using only the standard pediatric mathematical phantoms of 0, 1, 5, 10, and 15 years[27] could result in errors as large as 25%. In the present study, a patient-specific Monte Carlo calculation of the effective dose was set up, taking into account the exact irradiation geometry of the x-ray tubes and x-ray exposure settings used for a particular projection in a patient. Patient anatomy was simulated by an anthropomorphic phantom that was based on the gender and length of the patient.

For diagnostic cardiac catheterizations, a median effective dose of 4.6 mSv was found. Therapeutic procedures resulted in a higher median effective dose of 6.0 mSv because of the prolonged use of fluoroscopy and the larger number of cine runs. The reported values are as high as those for a typical adult cardiac angiography.[30] In ASD closure procedures, a significantly lower effective dose (median, 2.8 mSv) was found compared with the patent ductus arteriosus occlusions (median, 7.6 mSv) and balloon dilatations (median, 8.1 mSv). This can be attributed to the higher degree of difficulty for the cardiologist in those 2 procedures.[11] Moreover, for ASD closure, the cardiologist relied more on transesophageal imaging than on cine, resulting in a low effective dose. Overall, large variations in effective doses were found for diagnostic and therapeutic procedures, mostly because of differences in the difficulty level among individual patients. In only ≈10% of the cases, the effective dose was >20 mSv. Similar variations were found by Rassow et al,[21] who reported effective doses varying from ≈2 mSv (25th percentile) to ≈18 mSv (90th percentile) in infants. The same authors state that at least 50% of the effective dose was due to cineangiography. Schueler et al[10] calculated that cine made up 44% of the total exposure. Results from both studies are confirmed in our study, in which a median of 69% and 45% of the effective dose was attributed to cineangiography for diagnostic and therapeutic procedures, respectively. In both diagnostic and therapeutic procedures, the lateral and frontal tube exposures each contributed ≈50% to the total effective dose. An excellent correlation between the effective dose and the DAP was found ($r=0.95$), indicating that using a simple conversion coefficient (mSv/cGycm^2) to estimate effective dose is an acceptable way to calculate effective doses. Even when raw DAP data (without additional corrections) are used, the correlation remains good ($r=0.87$). Hence, a DAP meter is suitable for online estimation of the effective dose with good accuracy.

Using the risk factors from the multiplicative model of the ICRP,[19] we calculated an overall median risk of 0.08% (range, 0.007% to 0.481%). Because of the large variations in effective doses, no significant difference in risk could be shown between therapeutic and diagnostic procedures. The overall correlation between radiation risk and patient age was poor ($r=0.22$). However, a much higher median risk estimate was found for patients 0 to 1 year of age (0.10%) compared with patients 2 to 5 years (0.08%) and 6 to 10 years (0.05%) of age. Similar conclusions were presented by Rassow et al,[21] who found a significant increase in effective dose with decreasing age.

Because effective doses in pediatric cardiac catheterizations are high, dose reduction techniques should be applied to keep the dose as low as reasonably achievable and to reduce the radiation risks. Today, several techniques are available to decrease radiation exposure. Techniques that do not deteriorate image quality are of particular interest.

The introduction of pulsed fluoroscopy in the late 1980s resulted in a reduction in the radiation exposure rate of 30% to 50%.[10] In addition, the use of increased x-ray tube filtration removes lower-energy x-ray photons from the beam, thus reducing the amount of x-rays absorbed by the patient. In the present study, the dose-saving effect of an extra 0.2 mm copper beam filtration was demonstrated. With this low-dose

fluoroscopy, a significant reduction in the fluoroscopy dose was measured. The overall effect was an effective dose reduction of 18%. Contrast-detail analysis showed that this dose reduction was not detrimental to image quality.

Similar results were obtained by Baldazzi et al,[9] who used a foil of 0.1 mm of gadolinium. In their experimental setting, a mean reduction in effective dose/frame of 14% was reported while image quality was maintained. Other attempts to reduce the radiation dose such as the use of digital zooming (acquisition zoom) also resulted in a dose reduction. However, a significant deterioration in image quality was observed with this technology.[17]

In conclusion, skin doses are not problematic in pediatric interventional cardiology, but the calculated effective doses are as high as those for adult interventional cardiology, resulting in higher radiation risks. Therefore, it is important to monitor the patient dose by DAP instrumentation and to use additional beam filtration to keep the effective dose as low as possible in view of the age-related sensitivity of pediatric patients. Being a simple quantity, DAP readings can easily be included in patient records, especially those of young patients. The cumulative DAP (and hence effective dose) can be useful in decisions on the clinical management of the patient in case of follow-up examinations. Moreover, diagnostic reference levels of DAP could be useful for keeping the dose as low as possible and would be very valuable in training new interventional cardiologists.

References

1. den Boer A, de Feijter PJ, Serruys PW, et al. Real-time quantification and display of skin radiation during coronary angiography and intervention. *Circulation*. 2001;104:1779–1784.
2. Bakalyar DM, Castellani MD, Safian RD. Radiation exposure to patients undergoing diagnostic and interventional cardiac procedures. *Cathet Cardiovasc Diagn*. 1997;42:121–125.
3. Lobotessi H, Karoussou A, Neofotistou V, et al. Effective dose to a patient undergoing coronary angiography. *Radiat Prot Dosimetry*. 2001; 94:173–176.
4. Vaño E, Arranz L, Sastre JM, et al. Dosimetric and radiation protection considerations based on some cases of patient skin injuries in interventional cardiology. *Br J Radiol*. 1998;71:510–516.
5. Van de Putte S, Verhaegen F, Taeymans Y, et al. Correlation of patient skin doses in cardiac interventional radiology with dose-area product. *Br J Radiol*. 2000;73:504–513.
6. US Food and Drug Administration. Avoidance of serious X-ray-induced skin injuries to patients during fluoroscopically-guided procedures. *Med Bull*. 1994;24:7–17.
7. Fletcher DW, Miller DL, Balter S, et al. Comparison of four techniques to estimate radiation dose to skin during angiographic and interventional radiology procedures. *J Vasc Interv Radiol*. 2002;13:391–397.
8. European Community Council Directive 97/43Euratom of 30 June 1997 on health protection of individuals against the dangers of ionizing radiation in relation to medical exposure. *Off J*. 1997;L180:22–27.
9. Baldazzi G, Corazza I, Rossi PL, et al. In vivo effectiveness of gadolinium filter for paediatric cardiac angiography in terms of image quality and radiation exposure. *Phys Med*. 2002;18:109–113.
10. Schueler BA, Julsrud PR, Gray JE, et al. Radiation exposure and efficacy of exposure-reduction techniques during cardiac catheterization in children. *Am J Roentgenol*. 1994;162:173–177.
11. Allen HD, Driscoll DJ, Fricker FJ, et al. Guidelines for pediatric therapeutic cardiac catheterization: a statement for health professionals from the Committee on Congenital Cardiac Defects of the Council on Cardiovascular Disease in the Young, the American Heart Association. *Circulation*. 1991;84:2248–2258.
12. Boothroyd A, McDonald E, Moores BM, et al. Radiation exposure to children during cardiac catheterization. *Br J Radiol*. 1997;70:180–185.
13. Martin EC, Arthur MA, Olson P, et al. Radiation exposure to the pediatric patient during cardiac catheterization and angiocardiography: emphasis on the thyroid gland. *Circulation*. 1981;64:153–158.
14. Waldman JD, Rummerfield PS, Gilpin EA, et al. Radiation exposure to the child during cardiac catheterization. *Circulation*. 1981;64:158–163.
15. Li LB, Kai M, Kusama T. Radiation exposure to patients during paediatric cardiac catheterization. *Radiat Prot Dosimetry*. 2001;94:323–327.
16. Martin EC, Olson A. Radiation exposure to the paediatric patient from cardiac catheterization and angiocardiography. *Br J Radiol*. 1980;53: 100–106.
17. Ross RD, Joshi V, Carravallah DJ, et al. Reduced radiation during cardiac catheterization of infants using acquisition zoom technology. *Am J Cardiol*. 1997;79:691–693.
18. Leibovic SJ, Fellows KE. Patient radiation exposure during pediatric cardiac catheterization. *Cardiovasc Intervent Radiol*. 1983;6:150–153.
19. ICRP. *Recommendations of the International Commission on Radiological Protection*. Oxford, UK: Pergamon Press; 1991. Publication 60.
20. Axelsson B, Khalil C, Lidegran M, et al. Estimating the effective dose to children undergoing heart investigations: a phantom study. *Br J Radiol*. 1999;72:378–383.
21. Rassow J, Schmaltz AA, Hentrich F, et al. Effective doses to patients from paediatric cardiac catheterization. *Br J Radiol*. 2000;73:172–183.
22. Thijssen MAO, Bijkerk KR, van der Burght RJM. *Manual Contrast-Detail Phantom CDRAD Type 2.0: Project Quality Assurance in Radiology*. St Radboud, Netherlands: Department of Radiology, University Hospital Nijmegen; 1998.
23. Vaño E, Guibelalde E, Fernández JM, et al. Patient dosimetry in interventional radiology using slow films. *Br J Radiol*. 1997;70:195–200.
24. Briesmeister JF. MCNP: A General Monte Carlo N-Particle Transport Code. Los Alamos, NM; 1997. Version 4B, LA-16252-M.
25. Verhaegen F, Nahum AE, Van de Putte S, et al. Monte Carlo modeling of kV x-ray units. *Phys Med Biol*. 1999;44:1767–1789.
26. Iles WJ. *The Computation of Bremsstrahlung X-Ray Spectra Over an Energy Range 15 keV to 300 keV*. London, UK: NRPB: 1987. NRPB report R204.
27. Christy M, Eckerman KF. Specific Absorbed Fractions of Energy at Various Ages from Internal Photon Sources. ORNL/TM-8381, Oak Ridge, Tenn: 1987
28. Rosenstein M. *Organ Doses in Diagnostic Radiology*. Washington, DC: US Department of Health, Education and Welfare, Bureau of Radiological Health; 1976. BRh Tech publication DA 76–8030.
29. Kerr GD, Eckerman KF. Neutron and photon fluence-to-dose conversion factors for active marrow of the skeleton. In: Proc. of the Fifth Symposium on Neutron Dosimetry; 1985; Luxembourg. Vol I, EUR 9762 EN, CEC.
30. UNSCEAR. Sources and effects of ionizing radiation: volume I, sources: annex D, medical radiation exposure. Report to the General Assembly of the United Nations; 2000; New York, NY.

Patient-Specific Dose and Radiation Risk Estimation in Pediatric Cardiac Catheterization

Klaus Bacher, Evelien Bogaert, Régine Lapere, Daniël De Wolf and Hubert Thierens

Circulation. 2005;111:83-89; originally published online December 20, 2004;
doi: 10.1161/01.CIR.0000151098.52656.3A
Circulation is published by the American Heart Association, 7272 Greenville Avenue, Dallas, TX 75231

Print ISSN: 0009-7322. Online ISSN: 1524-4539